# Remote Biodegradation of Ge–Imogolite Nanotubes Controlled by the Iron Homeostasis of Pseudomonas brassicacearum

Astrid Avellan, Melanie Auffan, Armand Masion, Clément Levard, Marie Bertrand-Huleux, Jérôme Rose, Catherine Santaella, Wafa Achouak

# Remote Biodegradation of Ge−Imogolite Nanotubes Controlled by the Iron Homeostasis of *Pseudomonas brassicacearum*

Astrid Avellan,*[,†,‡,§] Melanie Auffan,[†,‡] Armand Masion,[†,‡] Clément Levard,[†,‡] Marie Bertrand,[§] Jérôme Rose,[†,‡] Catherine Santaella,[‡,§] and Wafa Achouak[‡,§]

[†]Aix-Marseille Université, CNRS, IRD, CEREGE UM34, 13545 Aix en Provence, France

[‡]iCEINT, International Consortium for the Environmental Implications of NanoTechology, CNRS, Duke University, Europôle de l'Arbois, 13545 Aix-en-Provence, France

[§]Laboratory of Microbial Ecology of the Rhizosphere and Extreme Environments (LEMIRE), Aix-Marseille Université, CEA, CNRS, UMR 7265 Biosciences and Biotechnology Institute of Aix-Marseille (BIAM), ECCOREV FR 3098, CEA/Cadarache, 13108 St-Paul-lez-Durance, France

ABSTRACT: The toxicity of high-aspect-ratio nanomaterials (HARNs) is often associated with oxidative stress. The essential nutrient Fe may also be responsible of oxidative stress through the production of reactive oxygen species. In the present study, it has been examined to what extent adding Fenton reaction promoting Fe impacted the toxicity of an alumino-germanate model HARN. Structural addition of only 0.95% wt Fe to Ge−imogolite not only alleviated the toxicity observed in the case of Fe-free nanotubes but also stimulated bacterial growth. This was attributed to the metabolization of siderophore-mobilized Fe from the nanotube structure. This was evidenced by the regulation of the homeostasis-monitoring intracellular Fe levels. This was accompanied by a biodegradation of the nanotubes approaching 40%, whereas the Fe-free nanomaterial remained nearly untouched.

## INTRODUCTION

In the aftermath of the asbestos crisis, the toxicity of fiber- and needle-shaped materials in general, and high-aspect-ratio nanotubes (HARNs) in particular, has drawn particular attention. In this context, positive and negative correlations have been described in the literature between the aspect ratio of several nanostructures and their ecotoxicity toward prokaryote cells,[1−4] reactive oxygen species (ROS) generation being the prevalent toxicity mechanism. Oxidative stress is not necessarily associated with the presence of a toxicant; intracellular Fe(II) is a known source of hydroxyl radicals as a product of the Fenton reaction.[5]

Iron is an essential nutrient with a pivotal role in bacterial metabolism growth and enzymatic reactions (e.g., Krebs cycle, nitrogen fixation, and DNA and metabolites synthesis).[6,7] Fe uptake by bacteria can occur for example through heme[8] or even directly in the form of ferrous Fe.[9] Siderophores, i.e., low-molecular-weight Fe chelators (400 to 1000 Da) produced by bacteria during Fe starvation, are involved in Fe(III) chelation, transport, internalization, and solubilization inside bacteria cells.[10−12]

Fe homeostasis within the cell regulates the Fe at levels promoting growth while preventing ROS-induced toxicity. Fe homeostasis involves complex genetic regulations that have been partly elucidated in several bacteria species. In most cases, the Fur (ferric uptake regulator) protein[13] has been identified as a regulator of the transcription of genes encoding for Fe uptake,[14] for Fe-using proteins,[15] or for protection against oxidative stress.[16] Therefore, Fe associated with nanomaterials (NM) in a form that can be internalized or released may have serious consequences on the intracellular Fe balance as well as ROS generation[17] and thus modify any existing toxicity.

It is a challenge to unequivocally distinguish the biophysico-chemical effects, both positive and negative, due to associated and added Fe. To a large extent, this is due to the difficulty of adding Fe to a material without any other modifications in chemistry and structure, including the purity of the product. This is particularly true when considering limited Fe addition, viz. doping, of HARNs in which the aspect ratio is one of the main material characteristics.

To circumvent these issues, we used Ge−imogolite as the model HARN in the present study. Ge−imogolite is isostructural to the naturally occurring alumino-silicate imogolite mineral and consists of a gibbsite tube wall curved by $GeO_4$ tetrahedra inside the tube. Its aqueous sol−gel

synthesis is byproduct-free and allows control over tube length[18] and diameter,[19] as well as the extent of structural defects,[20] making this nanotube a good model for the assessment of HARN nanotoxicity. There are already data regarding the toxicity of these model nanotubes concerning the diameter effect toward skin fibroblast,[21] length effects toward mouse lungs,[22] and structural defect effects toward *Pseudomonas brassicacearum*.[23] Iron doping of double-wall Ge−imogolite tubes (ca. 0.95% wt Fe) was successfully achieved by the structural substitution of Al in the tube wall, leaving other material parameters untouched.[24]

*P. brassicacearum* (strain NFM421), a Gram-negative soil bacterium isolated from the rhizosphere of *Arabidopsis thaliana*,[25] was chosen as the biological model for the present work because of its documented siderophore production in the form of pyoverdine and ornicorrugatin[26−28] and the knowledge of the mechanisms of its Fe regulation by the Fur protein. Indeed, the Fur regulation indirectly occurs via the repression of the noncoding RNAs (ncRNA) genes *prrF1* and *prrF2*.[14,29−31] Consequently, *prrF1* and *prrF2* genes are transcribed in *Pseudomonas* species during Fe starvation. Fur is also involved in the regulation of the pyoverdine biosynthesis via the negative regulation of genes encoding the pyoverdine synthase (*pvdL*) transcriptional factor.[32]

This choice of the system, viz. a model HARN with readily tunable chemistry, and bacteria whose Fe homeostasis mechanisms are known sets favorable conditions with which to investigate the effects of Fe on the biological responses. We followed a multidisciplinary approach to determine bacterial growth, ROS generation, Fe homeostasis regulation, and pyoverdine biosynthesis, as well as Fe biotransformation and bio distribution, for Ge−imogolite and Fe doped Ge−imo using two exposure modes.

## MATERIALS AND METHODS

**Ge−Imogolite.** Ge−imogolite and ca. 0.95% wt Fe-doped Ge−imogolite nanotubes (hereafter named, respectively, Ge−imo and Fe−imo) were synthesized as described previoulsy.[24] Briefly, tetraethyl orthogermanate was added to solutions of aluminum perchlorate (Ge−imo synthesis) or aluminum and ferrous perchlorate (Fe−imo synthesis). The $(n_{Al}+n_{Fe})/n_{Ge}$ molar ratio was set to 1.75, with an initial [Al]+[Fe] concentration of 0.5 mol $L^{-1}$. Al, Fe, and Ge were slowly hydrolyzed by the addition of 0.5 mol $L^{-1}$ NaOH. Growth of the nanotubes was performed at 95 °C for 7 days, and the resulting suspension was dialyzed against ultrapure water. The shape (length and diameter), crystallinity, chemical composition, and Fe-binding environment have been characterized using atomic-force microscopy (AFM), X-ray diffraction (XRD), inductively coupled plasma atomic emission spectroscopy (ICP-AES), and X-ray absorption spectroscopy (XAS), respectively.

**Bacterial Strain and Culture.** *P. brassicacearum* strain NFM421[25] was used to obtain NFM421::rfp genetically tagged with the red fluorescent protein (rfp) using a minTn5 cassette. This strain has been used previously, and no modification in bacterial physiology was observed.[26] NFM421::*rfp* harboring transcriptional *prrF1-gfp* fusion was obtained by inserting the pOT1e plasmid[33] presenting a gene coding for the green fluorescent protein (gfp) under the regulation of *prrF1* promoter region. Green fluorescence of the bacteria will then be a measure of the level of *prrF1* transcription.[34]

These strains from frozen stock (−80 °C) were grown on 10-fold diluted tryptic soil (Difco) broth solidified with 15 g $L^{-1}$ agar (TSA 1/10). A single colony was suspended in 10-fold diluted tryptic soil broth media (TSB 1/10) grown at 28 °C with stirring at 150 rpm until a concentration of $1 \times 10^9$ bacteria per mL was reached to be used as a preculture.

**Nanomaterials Exposure and Bacterial Growth.** The bacteria preculture suspensions were diluted to $1 \times 10^7$ bacteria per mL into the Fe-limited casamino acid (CAA) culture media (5 g $L^{-1}$ casamino acids, 1.18 g $L^{-1}$ dipotassium phosphate, and 0.25 g $L^{-1}$ magnesium sulfate). Bacteria control groups were grown in CAA or Fe-enriched CAA (100 $\mu$mol $L^{-1}$ $FeCl_3$, named CAA-Fe hereafter). Exposure of the bacteria to 50 mg $L^{-1}$ Ge−imo or Fe−imo was performed following two modes:

- direct contact (DC) between nanotubes and bacteria: cultures were made in (i) 200 $\mu$L CAA media in 96 well microplates (Greiner 96 flat-bottom black polystyrene) to follow bacterial growth or *prrF1* transcription or (ii) 150 mL CAA media in a sterile single-use Erlenmeyer flasks in polycarbonate (BD Falcon ) for chemical analyses; and
- no direct contact (NDC) between nanotubes and bacteria: Ge−imo or Fe−imo were added to 10 mL of CAA media and placed into a dialysis bag (DB) of 10 kDa pore size. This bag was then placed into a Erlenmeyer flasks (BD Falcon) containing 140 mL of CAA solution inoculated with $1 \times 10^7$ bacteria per mL.

Cultures were incubated at 28 °C on a shaker table (150 rpm) for 24 h in dark conditions. All experiments were made in triplicate. Bacterial growth was assessed by the counting of colony forming units (CFU $mL^{-1}$).

**Iron Homeostasis.** Iron homeostasis was assessed by analyzing the expression of the pyoverdine synthase gene *pvdL*, the pyoverdine induced fluorescence, as well as the Fe(II) intracellular level.

Total RNA was extracted from an overnight growth culture using the RNAprotect bacteria reagent kit (Qiagen). The reverse transcription was processed using the RT Roche transcriptor kit (Roche) using the HotStarTaq Polymerase (Qiagen). The primers used for the *pvdL* amplification were *pvdL-Forward* (5′-AATGGGCTGGTCTTGGCCGG-3′) and *pvdL-Reverse* (5′-AGCGTTGTTTGCCCAGACGC-3′)

The presence of pyoverdine in the bacterial growth medium (NFM::rfp strain) was assessed by fluorescence measurements[35] ($\lambda_{ex}$: 473 nm; $\lambda_{em}$: 510 nm) using TECAN i-control spectrofluorimeter and was normalized by the number of CFU.

Fe(II) intracellular lever was assessed using the NFM421::rfp strain harboring transcriptional *prrF1-gfp* fusion, in which the gene encoding for the green fluorescent protein (gfp) was under the regulation of the *prrF1* promoter. Green fluorescence of each sample ($\lambda_{ex}$: 473 nm; $\lambda_{em}$: 510 nm) was measured using TECAN i-control spectrofluorimeter and was normalized by the number of CFU $mL^{-1}$. The green fluorescence intensity per cell was expressed as a proportion of the fluorescence of the control group (100%).

**Reactive Oxygen Species.** Accumulation of ROS in cells was estimated using the nonfluorescent DCFDA (2′,7′-dichlorodihydrofluorescein diacetate) probe. Precultures of NFM421::rfp were centrifuged at 12000g for 2 min, washed three times with CAA, and finally suspended in 500 $\mu$L of CAA containing 500 $\mu$mol $L^{-1}$ DCFDA. The suspension was electroporated in 1 mm wide cuvettes at 25 $\mu$F, 2.5 kV, and

200 Ω for 5 ms (Multiporator, Eppendorf, Germany). The electroporated cells were divided into fractions, diluted at $10^7$ cells $mL^{-1}$ in the CAA and CAA−Fe media for the control groups, or exposed to 25 mmol $L^{-1}$ $H_2O_2$ (positive control), 50 mg $L^{-1}$ of Ge−imo, or 50 mg $L^{-1}$ of Fe−imo at 28 °C for 15 min.

Upon crossing the cell membranes, DCFDA acetate groups are removed by an intracellular esterase. In the presence of ROS, the probe is oxidized into a green-fluorescent form (DCF). The samples were observed using a confocal microscope (Olympus Fluoview FV10i). DCF ($\lambda_{ex}$= 490 nm, $\lambda_{em}$= 527 nm) and RFP (bacteria) ($\lambda e_x$= 559 nm, $\lambda_{em}$= 569 nm) signals were monitored. At least 1000 red or green cells were counted on at least five different pictures using the ImageJ 1.49 software[36] to calculate the ratio of DCF-labeled cells.

**Biotransformation and Biodistribution.** Al, Ge, and Fe concentrations were used as proxies of Ge−imo and Fe−imo degradation. These concentrations were measured with an inductively coupled plasma mass spectrophotometer (ICP-MS, NexION 350, PerkinElmer) after overnight acid digestion with 70% $HNO_3$ 3:1 (v/v) and dilution with ultrapure water on samples of nanomaterial inside the dialysis bag and biotic or abiotic media outside the dialysis bag.

Nanomaterial biodegradation and interaction with bacteria were studied using enhanced darkfield microscope (Olympus BX51) equipped with a CytoViva HyperSpectral Imaging (HSI) system (Auburn, AL). A drop (20 μL) of sample was deposited on a clean glass slide and covered with a coverslip for imaging. Pictures were made by using 75% light magnification and 0.25 s acquisition time per line. Hyperspectral signal acquisition was processed in each pixel following light absorption for wavelengths from 400 to 1000 nm with a 1.3 nm step. Each pixel thus has a spectral signature modulated by the nature of the material.[37] A spectral library was built using pictures of the nanomaterial in abiotic culture media after 24 h. Once checked for their specificity, these NM spectral libraries were used to process a spectral angle mapper (SAM) on hyperspectral pictures using a maximum angle of 0.085 rad. Analyses were performed using the ENVI 5.1 software (exelis). Each pixel on pictures containing the spectral signature of the nanomaterial was labeled with a specific color (see the Supporting Information for more details).

## RESULTS AND DISCUSSION

**Synthesis of Ge−Imogolite and Fe-Doped Ge−Imogolite.** The synthesis yielded in double-walled Ge−imogolite nanotubes of 60 ± 30 nm in length and 3.5 ± 0.5 nm in diameter. Fe−imo was obtained by structurally substituting Al for Fe in the tube walls and leading to an adjacent vacancy, as observed earlier.[24] The Fe amount in the Fe−imo tubes was 0.95% wt, and the suspension was free of co-precipitated forms of Fe (e.g., Fe oxy- and hydroxide).

**Biodistribution and Toxicity of the Nanotubes.** Figure 1 summarizes the growth at 24 h of *P. brassicacearum* in the control-media CAA and CAA−Fe, as well as after exposure to Ge−imo and Fe−imo in both DC and NDC scenarios. As expected, the enhanced growth observed in CAA−Fe compared to CAA is the result of the increased amount of bioavailable Fe.[38]

Compared to the results from the CAA control, the only occurrence of significant growth reduction was exposure to Ge−imo in the DC mode, in which the number of CFU is lower by approximately 1 order of magnitude. When contact

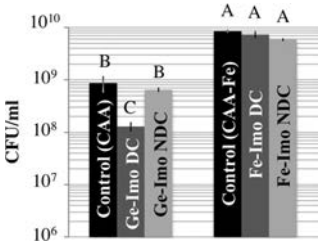


**Figure 1.** Colony-forming units (CFU) of *P. brassicacearum*, NFM421::rfp strain after 24 h growth in CAA or CAA−Fe, exposed to 50 mg $L^{-1}$ Ge−imogolite (Ge−imo) or Fe−imogolite (Fe−imo). Interactions between the nanotubes and the bacteria with direct contact (DC) or without direct contact (NDC). Groups showing different letters are significantly different. (ANOVA, followed by Tukey's HSD test, $p < 0.05$). Error bars represent the confidence interval ($\alpha = 0.05$).

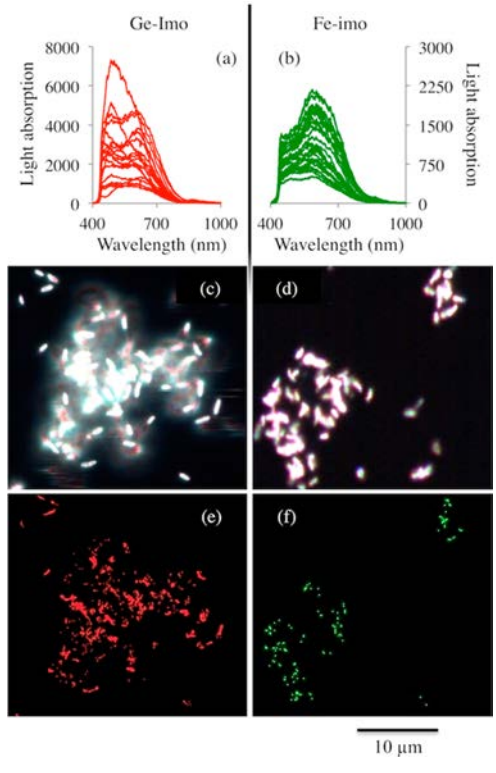


**Figure 2.** Hyperspectral imaging of 50 mg $L^{-1}$ Ge−imo and Fe−imo in direct contact with the *P. brassicacearum* NFM421::rfp strain after 24 h of growth. Images were acquired using a 100× objective and 1.3 oil iris. Reference spectral libraries of (a) Ge−imo and (b) Fe−imo created in CAA. Hyperspectral scanned images of bacteria exposed to (c) Ge−imo and (d) Fe−imo and their respective localization, (e) and (f), were obtained using Spectral Angle Mapper. Illuminated pixels have spectral signatures identical to those in the respective spectral libraries.

was prevented (NDC scenario), Ge−imo did not cause any significant inhibition of the bacterial growth (Figure 1). This suggests that the sorption of Ge−imo on bacterial cells may damage membranes or lower the growth rate. This is consistent with previous studies, showing that the contact between the nanomaterial and the cells led to toxic effects.[39−42] In the present case, the contact between Ge−imo and the bacteria was confirmed by the presence of heteroaggregates detected by enhanced dark-field microscopy coupled to HSI (Figure 2). The growth inhibition observed for Ge−imo in the DC mode is

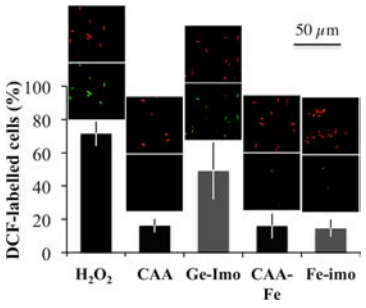


**Figure 3.** ROS quantification inside the *P. brassicacearum*, NFM421::rfp strain. Top images: RFP fluorescence (all bacteria). Bottom images: DFC fluorescence (presence of intracellular ROS, Materials and Methods section). Bacteria were exposed to 25 mmol $L^{-1}$ $H_2O_2$ (positive control), CAA or CAA-Fe (controls), and 50 mg $L^{-1}$ of Ge−imo or Fe−imo (DC mode). Error bars represent confidence intervals ($\alpha$ = 0.05).

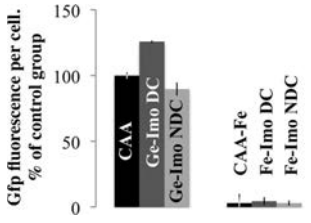


**Figure 4.** *prrF1* expression regulation in *P. brassicacearum*. The gfp signal was normalized by the number of bacteria per mL. Results are expressed in percentage of the control (CAA). Bacteria were exposed for 24 h to 50 mg $L^{-1}$ of Ge−imo or Fe−imo in DC and NDC exposure modes. Error bars represent confidence intervals ($\alpha$ = 0.05).

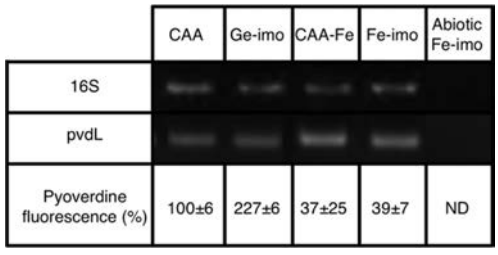


**Figure 5.** Transcription of *pvdL* and quantification of pyoverdine. *P. brassicacearum* was grown in CAA and CAA−Fe or exposed to 50 mg $L^{-1}$ of Ge−imo or Fe−imo using the direct contact mode. The expression of *pvdL* and 16S RNA was analyzed by RT-PCR. Pyoverdine fluorescence was normalized by the number of bacteria per mL. Standard deviations are based on triplicates.

associated with a significant increase of the proportion of ROS containing cells (up to 50%) (Figure 3). This is in agreement with other nanotoxicity studies reporting oxidative stress of a main toxicity mechanism.[39,43]

Exposure of *P. brassicacearum* to Fe−imo in both the DC and the NDC scenarios resulted in bacterial growth similar to that in the CAA−Fe control, i.e., enhanced growth compared to that in the equivalent experiments with Ge−imo (Figure 1). As opposed to Ge−imo, the proportion of ROS-containing cells after exposure to Fe−imo did not exceed the one of the CAA control (Figure 3). Fe added as $FeCl_3$ in the CAA−Fe medium had no detectable effect on the ROS production either (Figure 3). This indicates that in the present systems, Fe had no detrimental effects in terms of toxicity, regardless of the form in which it was added to the culture medium (Fe−imo or $FeCl_3$ probably precipitated into FeOOH phases).

Although direct contact was a condition in which to observe diminished growth with Ge−imo, the formation of hetero-aggregates in the case of Fe−imo had no negative repercussions (Figures 2 and 3). As a matter of fact, the presence of Fe in the Fe−imo not only alleviated the toxicity but also favored bacterial growth to the level observed in the Fe-supplemented culture medium regardless of the exposure mode (Figure 1). This observation suggests that bacteria were able to use the Fe incorporated within the Fe−imo for their metabolism under the control of a mechanism capable of mobilizing remote iron.

**Disturbance of the Iron Homeostasis in Bacteria Exposed to the Nanotubes.** The differences in bacterial growth and ROS production observed after exposure to Ge−imo or Fe−imo demonstrate that Fe plays a key role in the effects of these nanotubes toward *P. brassicacearum*. The above-stated assumption that the iron within the tube walls of Fe−imo participates in the Fe metabolism of the cells should have consequences on the Fe homeostasis.

The Fe(II) homeostasis in *Pseudomonas* species is regulated by the Fur binding protein and the ncRNAs *prrF1* and *prrF2*, which can be base-paired with specific mRNAs, inhibiting the translation of genes encoding for nonessential Fe-using proteins.[15] At high intracellular Fe(II) content, Fe(II) binds to the Fur protein, which represses the expression of *prrF1* and *prrF2*.[14,29,31] Under Fe starvation, the transcription of *prrF* genes resumes, leading to their expression. Consequently, the ncRNA *prrF1* can be used as an indicator of intracellular Fe(II) level.

Figure 4 displays the normalized gfp fluorescence signal for all experiments. As expected, the Fe-supplemented culture medium displayed a decreased gfp fluorescence compared to that in the CAA control, indicating the availability of Fe above starvation levels and thus an increase of intracellular Fe. This is consistent with the observed improved growth in the CAA-Fe medium (Figure 1).

Exposure to Ge−imo had no effect toward the *prrF1* transcription regulation (gfp level per cell 90%) when contact between nanotubes and bacteria was prevented (Figure 4). A significant increase of *prrF1* transcription was observed when bacteria and Ge−imo were in contact, indicating a decrease in intracellular Fe(II). Because exposure to Ge−imo led to intracellular ROS production, this decrease of the intracellular Fe(II) is consistent with a defense mechanism in which which Fe(II) is released from the cells or Fe(III) uptake is halted to prevent damages from the Fenton reaction.[5,44]

Exposure of *P. brassicacearum* to the Fe-doped imogolite tubes resulted in a drastic decrease of the gfp fluorescence, and thus an increase of intracellular Fe(II), for both the DC and the NDC scenarios. It is useful to remember here that the iron introduced in the system is the Fe(III) in the tube walls of Fe−imo in the absence of any other Fe form.[24] The observed increase of Fe content in the cells (Figure 4) supports the assumption that the bacteria were able to take up the Fe atoms from the structure of the Fe−imo and to solubilize at least a part of it within the cells. The amplitude of the decrease of the gfp fluorescence is identical (within the margin of error) in both exposure modes, thereby suggesting that the same Fe-uptake mechanism was involved. Considering that Fe mobilization from the Fe−imo structure needs to occur also at a distance (viz. NDC exposure mode), plausible mechanisms by which to transport Fe into the cell are either in the form of

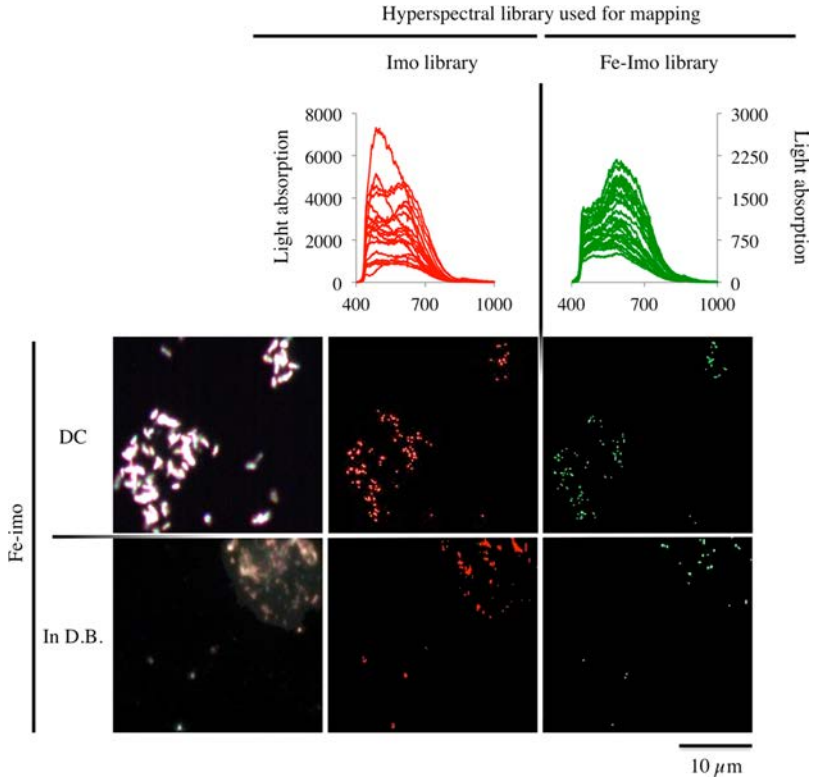


**Figure 6.** Fe−imogolite (Fe−imo) alteration after 24 h of exposure to bacteria following the DC and NDC scenarios. Fe−imo were (top panel) in contact with *P. brassicacearum* and (bottom panel) isolated inside a dialysis bag (DB). Spectral Angle Mapper (angle: 0.85 rad) was processed using the Ge−imo or Fe−imo spectral libraries. Illuminated pixels show hyperspectral signatures similar to spectral libraries.

ionic Fe after the prior dissolution of the structure, as previously observed in the case of Fe-doped ZnO,[45] or in chelated form via the siderophores produced by the bacteria.

**Structural Transformation of the Nanotubes.** The evolution of the structural integrity of the nanotubes was assessed by measuring the Al, Fe, and Ge released from the Ge−imo and Fe−imo tubes. To avoid sampling and separation issues, we limited these determinations to the NDC experiments. Al, Ge, and Fe concentrations were measured inside and outside the dialysis bag to calculate the percentage of release (see Figure S2). The elements crossing the 10 kDa dialysis membrane were assumed to be dissolved in ionic or chelated form. In abiotic CAA, element release was in a 6.3 ± 0.2% to 13.6 ± 0.9% range for all tubes, indicating the limited degradation of the nanomaterial. In the case of Ge−imo, the proportion of released elements in the presence of *P. brassicacearum* was quasi-identical to the abiotic system. Although the released quantities of Al and Ge reached levels of documented toxicity toward bacteria,[46,47] they had no effects on bacterial growth in the present systems (Figure 1), probably due to favorable Al and Ge speciation in terms of toxic effects.

Drastic tube degradation was observed for Fe−imo in the biotic system: in the presence of bacteria, the release of Al and Ge from the Fe−imo structure approached 40%. This proportion reached 90% for Fe. Dissolution and chelation by CAA components caused the release of ca. 10% of the Fe under abiotic conditions. The nearly complete release of Fe under biotic condition is consequently attributable to chelation controlled by bacterial activity, i.e., the production of siderophores.

The production of the pyoverdine siderophore was assessed by its fluorescence and by monitoring the pyoverdine synthase-encoding gene (*pvdL*). The transcription of *pvdL* occurred in all cases of exposure because of the Fe deficit in the culture medium (Figure 5). Compared to that in the system without nanomaterial, the pyoverdine fluorescence (normalized by bacteria concentration) increased significantly upon exposure of *P. brassicacearum* to Ge−imo (Figure 5), indicating iron starvation, in agreement with the increased *prrF1* expression (Figure 4). When Fe was added to the medium in the form of $FeCl_3$ or Fe−imo, the biosynthesis of pyoverdine by *P. brassicacearum* decreased (Figure 5). The effective iron chelation and transport into the cells increased the intracellular Fe(II) levels (Figure 4), leading to a subsequent diminished pyoverdine production.[32]

This Fe chelation caused the disruption of the tube structure, as already evidenced by the release of approximately 40% of the Al and Ge. More-detailed insight into the degradation of the tubes was provided by HSI. Ge−imo and Fe−imo have distinct spectral signatures (cf. the Supporting Information). The images obtained after 24 of h exposure of the bacteria to Fe−imo in both DC and NDC show the presence of residual Fe−imo despite the 90% release of Fe from the tubes (Figure 6). The images also reveal the presence of Ge−imo, co-localized with the Fe−imo signal. This suggests partial and stepwise disruption of the tubes. The chelation of Fe from the Fe−imo structure produced Fe-free tube fragments whose spectral signature is the one recorded for Ge−imo (Figure 6). Because this is associated with a degradation of 40% of the tubes, this suggests that the HSI spectral signature is not strictly size-dependent.

Siderophore-mediated degradation of nanostructures has been reported previously for nanohematite.[48−50] The chelation efficiency of siderophores can be estimated via the stability

constants of their complexes with Fe: this constant is 32.5 (log K) for desferri-ferrioxiamin[51] and even higher for cathecholate siderophores.[52] As a comparison, the stability constant for Fe(III)-EDTA complex is only 25.7.[51] Although Al and Ge may be complexed by siderophores,[53,54] there is no evidence of this phenomenon in the present study: the strongest pyoverdine production was observed in the case of exposure to Ge–imo, but this was not linked to increased release of Al or Ge.

In the case of the Fe–imo nanotubes, the vacancies adjacent to Fe in the wall structure[24] may have facilitated the chelation of iron by the siderophore and the subsequent tube disruption due to structure-weakening defects.

**Environmental Implications.** Reports on the chelation-mediated biodegradation of nanostructures are rather scarce,[55] although these phenomena received some attention in the case of iron nanomaterials.[48–50,56,57] In a non-nanospecific context, siderophores produced by a variety of organisms[58,59] are known to play a role in the chelation and dissolution of various elements and mineral phases.[54,58,60–62] In the present study, this type of metabolic response resulted in the reversal of the toxicity of a model HARN by simply adding Fe amounts below the single-digit percentage range to the structure of the nanomaterial. This demonstrates that elements in the concentration range of impurities, present whether by design or by accident, are likely to have significant effects on the toxicity and the biodegradation of nanomaterials. In a simply mechanistic approach as well as in a regulatory context, the present results demonstrate the difficulty of defining and implementing meaningful toxicity-testing strategy.

## ASSOCIATED CONTENT

The Supporting Information is available at the end of the document. Figures showing hyperspectral images used for spectral libraries building and the tests necessary to ensure their specificity and concentrations of Al, Ge, and Fe used for the degradation percentage calculation. (PDF)

## AUTHOR INFORMATION

### Corresponding Author

*E-mail: avellan@cerege.fr.

### Notes

The authors declare no competing financial interest.

## ACKNOWLEDGMENTS

The authors acknowledge the CNRS funding for the GDRi iCEINT and the OSU-Institut Pythéas. This work is a contribution to the Labex Serenade (ANR-11-LABX-0064) funded by the "Investissements d'Avenir" French Government program of the French National Research Agency (ANR) through the A*MIDEX project (ANR-11-IDEX-0001-02).

## REFERENCES

(1) Yang, C.; Mamouni, J.; Tang, Y.; Yang, L. Antimicrobial Activity of Single-Walled Carbon Nanotubes: Length Effect. *Langmuir* **2010**, *26* (20), 16013–16019.

(2) Simon-Deckers, A.; Loo, S.; Mayne-L'hermite, M.; Herlin-Boime, N.; Menguy, N.; Reynaud, C.; Gouget, B.; Carrière, M. Size-, composition- and shape-dependent toxicological impact of metal oxide nanoparticles and carbon nanotubes toward bacteria. *Environ. Sci. Technol.* **2009**, *43* (21), 8423–8429.

(3) Tong, T.; Shereef, A.; Wu, J.; Binh, C. T. T.; Kelly, J. J.; Gaillard, J.-F.; Gray, K. A. Effects of Material Morphology on the Phototoxicity of Nano-TiO2 to Bacteria. *Environ. Sci. Technol.* **2013**, *47* (21), 12486–12495.

(4) Le, T. T. A.; McEvoy, J.; Khan, E. The effect of single-walled carbon nanotubes on Escherichia coli: multiple indicators of viability. *J. Nanopart. Res.* **2015**, *17* (1), 1–9.

(5) Faulkner, M. J.; Helmann, J. D. Peroxide Stress Elicits Adaptive Changes in Bacterial Metal Ion Homeostasis. *Antioxid. Redox Signaling* **2011**, *15* (1), 175–189.

(6) Andrews, S. C.; Robinson, A. K.; Rodríguez-Quiñones, F. Bacterial iron homeostasis. *FEMS Microbiol. Rev.* **2003**, *27* (2–3), 215–237.

(7) Kadner, R. J. Regulation by iron: RNA rules the rust. *J. Bacteriol.* **2005**, *187* (20), 6870–6873.

(8) Wandersman, C.; Stojiljkovic, I. Bacterial heme sources: the role of heme, hemoprotein receptors and hemophores. *Curr. Opin. Microbiol.* **2000**, *3* (2), 215–220.

(9) Cartron, M. L.; Maddocks, S.; Gillingham, P.; Craven, C. J.; Andrews, S. C. Feo - Transport of ferrous iron into bacteria. *BioMetals* **2006**, *19* (2), 143–157.

(10) Pattus, F.; Abdallah, M. A. Siderophores and Iron-Transport in Microorganisms. *J. Chin. Chem. Soc.* **2000**, *47* (1), 1–20.

(11) Albrecht-Gary, A.-M.; Blanc, S.; Rochel, N.; Ocaktan, A. Z.; Abdallah, M. A. Bacterial Iron Transport: Coordination Properties of Pyoverdin PaA, a Peptidic Siderophore of Pseudomonas aeruginosa. *Inorg. Chem.* **1994**, *33* (26), 6391–6402.

(12) Cezard, C.; Farvacques, N.; Sonnet, P. Chemistry and Biology of Pyoverdines, Pseudomonas Primary Siderophores. *Curr. Med. Chem.* **2015**, *22* (2), 165–186.

(13) Escolar, L.; Pérez-Martín, J.; de Lorenzo, V. Opening the iron box: transcriptional metalloregulation by the Fur protein., Opening the Iron Box: Transcriptional Metalloregulation by the Fur Protein. *J. Bacteriol. J. Bacteriol.* **1999**, *181* (20), 6223–6229.

(14) Wilderman, P. J.; Sowa, N. A.; FitzGerald, D. J.; FitzGerald, P. C.; Gottesman, S.; Ochsner, U. A.; Vasil, M. L. Identification of tandem duplicate regulatory small RNAs in Pseudomonas aeruginosa involved in iron homeostasis. *Proc. Natl. Acad. Sci. U. S. A.* **2004**, *101* (26), 9792–9797.

(15) Hantke, K. Iron and metal regulation in bacteria. *Curr. Opin. Microbiol.* **2001**, *4* (2), 172–177.

(16) Becerra, G.; Merchán, F.; Blasco, R.; Igeño, M. I. Characterization of a ferric uptake regulator (Fur)-mutant of the cyanotrophic bacterium Pseudomonas pseudoalcaligenes CECT5344. *J. Biotechnol.* **2014**, *190*, 2–10.

(17) Turci, F.; Tomatis, M.; Lesci, I. G.; Roveri, N.; Fubini, B. The iron-related molecular toxicity mechanism of synthetic asbestos nanofibres: a model study for high-aspect-ratio nanoparticles. *Chem. - Eur. J.* **2011**, *17* (1), 350–358.

(18) Amara, M.-S.; Paineau, E.; Bacia-Verloop, M.; Krapf, M.-E. M.; Davidson, P.; Belloni, L.; Levard, C.; Rose, J.; Launois, P.; Thill, A. Single-step formation of micron long (OH)3Al2O3Ge(OH) imogolite-like nanotubes. *Chem. Commun.* **2013**, *49* (96), 11284–11286.

(19) Maillet, P.; Levard, C.; Larquet, E.; Mariet, C.; Spalla, O.; Menguy, N.; Masion, A.; Doelsch, E.; Rose, J.; Thill, A. Evidence of double-walled Al-Ge imogolite-like nanotubes. a cryo-TEM and SAXS investigation. *J. Am. Chem. Soc.* **2010**, *132* (4), 1208–1209.

(20) Levard, C.; Masion, A.; Rose, J.; Doelsch, E.; Borschneck, D.; Olivi, L.; Chaurand, P.; Dominici, C.; Ziarelli, F.; Thill, A.; et al. Synthesis of Ge-imogolite: influence of the hydrolysis ratio on the structure of the nanotubes. *Phys. Chem. Chem. Phys.* **2011**, *13* (32), 14516–14522.

(21) Liu, W.; Chaurand, P.; Di Giorgio, C.; De Méo, M.; Thill, A.; Auffan, M.; Masion, A.; Borschneck, D.; Chaspoul, F.; Gallice, P.; et al. Influence of the length of imogolite-like nanotubes on their cytotoxicity and genotoxicity toward human dermal cells. *Chem. Res. Toxicol.* **2012**, *25* (11), 2513–2522.

(22) van den Brule, S.; Beckers, E.; Chaurand, P.; Liu, W.; Ibouraadaten, S.; Palmai-Pallag, M.; Uwambayinema, F.; Yakoub, Y.;

Avellan, A.; Levard, C.; et al. Nanometer-long Ge-imogolite nanotubes cause sustained lung inflammation and fibrosis in rats. *Part. Fibre Toxicol.* **2014**, *11* (1), 67.

(23) Avellan, A.; Levard, C.; Rose, J.; Auffan, M.; Bertrand, M.; Olivi, L.; Santaella, C.; Achouak, W.; Masion, A. Influence of structural defects of Ge-imogolite nanotubes on their toxicity towards Pseudomonas brassicacearum. *Environ. Sci. Nano* **2016**, DOI: 10.1039/C6EN00060F.

(24) Avellan, A.; Levard, C.; Kumar, N.; Rose, J.; Olivi, L.; Thill, A.; Chaurand, P.; Borschneck, D.; Masion, A. Structural incorporation of iron into Ge−imogolite nanotubes: a promising step for innovative nanomaterials. *RSC Adv.* **2014**, *4* (91), 49827−49830.

(25) Achouak, W.; Sutra, L.; Heulin, T.; Meyer, J. M.; Fromin, N.; Degraeve, S.; Christen, R.; Gardan, L. Pseudomonas brassicacearum sp. nov. and Pseudomonas thivervalensis sp. nov., two root-associated bacteria isolated from Brassica napus and Arabidopsis thaliana. *Int. J. Syst. Evol. Microbiol.* **2000**, *50* (1), 9−18.

(26) Achouak, W.; Conrod, S.; Cohen, V.; Heulin, T. Phenotypic Variation of *Pseudomonas brassicacearum* as a Plant Root-Colonization Strategy. *Mol. Plant-Microbe Interact.* **2004**, *17* (8), 872−879.

(27) Meyer, J.-M.; Geoffroy, V. A.; Baida, N.; Gardan, L.; Izard, D.; Lemanceau, P.; Achouak, W.; Palleroni, N. J. Siderophore typing, a powerful tool for the identification of fluorescent and nonfluorescent pseudomonads. *Appl. Environ. Microbiol.* **2002**, *68* (6), 2745−2753.

(28) Matthijs, S.; Brandt, N.; Ongena, M.; Achouak, W.; Meyer, J.-M.; Budzikiewicz, H. Pyoverdine and histicorrugatin-mediated iron acquisition in Pseudomonas thivervalensis. *BioMetals* **2016**, *29*, 467−485.

(29) Massé, E.; Salvail, H.; Desnoyers, G.; Arguin, M. Small RNAs controlling iron metabolism. *Curr. Opin. Microbiol.* **2007**, *10* (2), 140−145.

(30) Reinhart, A. A.; Powell, D. A.; Nguyen, A. T.; O'Neill, M.; Djapgne, L.; Wilks, A.; Ernst, R. K.; Oglesby-Sherrouse, A. G. The prrF-Encoded Small Regulatory RNAs Are Required for Iron Homeostasis and Virulence of Pseudomonas aeruginosa. *Infect. Immun.* **2015**, *83* (3), 863−875.

(31) Sonnleitner, E.; Haas, D. Small RNAs as regulators of primary and secondary metabolism in Pseudomonas species. *Appl. Microbiol. Biotechnol.* **2011**, *91* (1), 63−79.

(32) Leoni, L.; Ciervo, A.; Orsi, N.; Visca, P. Iron-regulated transcription of the pvdA gene in Pseudomonas aeruginosa: effect of Fur and PvdS on promoter activity. *J. Bacteriol.* **1996**, *178* (8), 2299−2313.

(33) Allaway, D.; Schofield, N. A.; Leonard, M. E.; Gilardoni, L.; Finan, T. M.; Poole, P. S. Use of differential fluorescence induction and optical trapping to isolate environmentally induced genes. *Environ. Microbiol.* **2001**, *3* (6), 397−406.

(34) Utratna, M.; O'Byrne, C. P. Using enhanced green fluorescent protein (EGFP) promoter fusions to study gene regulation at single cell and population levels. *Methods Mol. Biol.* **2014**, *1157*, 233−247.

(35) Sosnin, E. A.; Zhdanova, O. S.; Kashapova, E. R.; Artyukhov, V. Y. Pyoverdine as a fluorescent marker of antibiotic sensitivity of Pseudomonas Aeruginosa. *Opt. Spectrosc.* **2014**, *117* (6), 1018−1024.

(36) Abramoff, M. D.; Magalhães, P. J.; Ram, S. J. Image processing with ImageJ. *Biophotonics Int.* **2004**, *11* (7), 36−42.

(37) Badireddy, A. R.; Wiesner, M. R.; Liu, J. Detection, Characterization, and Abundance of Engineered Nanoparticles in Complex Waters by Hyperspectral Imagery with Enhanced Darkfield Microscopy. *Environ. Sci. Technol.* **2012**, *46* (18), 10081−10088.

(38) Loper, J. E.; Lindow, S. E. A biological sensor for iron available to bacteria in their habitats on plant surfaces. *Appl. Environ. Microbiol.* **1994**, *60* (6), 1934−1941.

(39) Djurišić, A. B.; Leung, Y. H.; Ng, A. M. C.; Xu, X. Y.; Lee, P. K. H.; Degger, N.; Wu, R. S. S. Toxicity of Metal Oxide Nanoparticles: Mechanisms, Characterization, and Avoiding Experimental Artefacts. *Small* **2015**, *11* (1), 26−44.

(40) Thill, A.; Zeyons, O.; Spalla, O.; Chauvat, F.; Rose, J.; Auffan, M.; Flank, A. M. Cytotoxicity of CeO2 nanoparticles for Escherichia coli. Physico-chemical insight of the cytotoxicity mechanism. *Environ. Sci. Technol.* **2006**, *40* (19), 6151−6156.

(41) Applerot, G.; Lipovsky, A.; Dror, R.; Perkas, N.; Nitzan, Y.; Lubart, R.; Gedanken, A. Enhanced Antibacterial Activity of Nanocrystalline ZnO Due to Increased ROS-Mediated Cell Injury. *Adv. Funct. Mater.* **2009**, *19* (6), 842−852.

(42) Jiang, W.; Yang, K.; Vachet, R. W.; Xing, B. Interaction between oxide nanoparticles and biomolecules of the bacterial cell envelope as examined by infrared spectroscopy. *Langmuir* **2010**, *26* (23), 18071−18077.

(43) von Moos, N.; Slaveykova, V. I. Oxidative stress induced by inorganic nanoparticles in bacteria and aquatic microalgae − state of the art and knowledge gaps. *Nanotoxicology* **2014**, *8* (6), 605−630.

(44) Cornelis, P. Iron uptake and metabolism in pseudomonads. *Appl. Microbiol. Biotechnol.* **2010**, *86* (6), 1637−1645.

(45) Li, M.; Pokhrel, S.; Jin, X.; Mädler, L.; Damoiseaux, R.; Hoek, E. M. V. Stability, Bioavailability, and Bacterial Toxicity of ZnO and Iron-Doped ZnO Nanoparticles in Aquatic Media. *Environ. Sci. Technol.* **2011**, *45* (2), 755−761.

(46) Wood, M. A mechanism of aluminium toxicity to soil bacteria and possible ecological implications. *Plant Soil* **1995**, *171* (1), 63−69.

(47) Slawson, R. M.; Van Dyke, M. I.; Lee, H.; Trevors, J. T. Germanium and silver resistance, accumulation, and toxicity in microorganisms. *Plasmid* **1992**, *27* (1), 72−79.

(48) Dehner, C. A.; Barton, L.; Maurice, P. A.; DuBois, J. L. Size-Dependent Bioavailability of Hematite ($\alpha$-Fe2O3) Nanoparticles to a Common Aerobic Bacterium. *Environ. Sci. Technol.* **2011**, *45* (3), 977−983.

(49) Barton, L. E.; Quicksall, A. N.; Maurice, P. A. Siderophore-Mediated Dissolution of Hematite ($\alpha$-Fe2O3): Effects of Nanoparticle Size. *Geomicrobiol. J.* **2012**, *29* (4), 314−322.

(50) Dehner, C.; Morales-Soto, N.; Behera, R. K.; Shrout, J.; Theil, E. C.; Maurice, P. A.; Dubois, J. L. Ferritin and ferrihydrite nanoparticles as iron sources for Pseudomonas aeruginosa. *JBIC, J. Biol. Inorg. Chem.* **2013**, *18* (3), 371−381.

(51) Furia, T. E. Sequestrants in Foods. In *CRC Handbook of Food Additives*, 2nd ed.; CRC Press: Boca Raton, FL, 1973.

(52) Brantley, S. L.; Liermann, L.; Bullen, T. D. Fractionation of Fe isotopes by soil microbes and organic acids. *Geology* **2001**, *29* (6), 535.

(53) del Olmo, A.; Caramelo, C.; SanJose, C. Fluorescent complex of pyoverdin with aluminum. *J. Inorg. Biochem.* **2003**, *97* (4), 384−387.

(54) Baramov, T.; Keijzer, K.; Irran, E.; Mösker, E.; Baik, M.-H.; Süssmuth, R. Synthesis and Structural Characterization of Hexacoordinate Silicon, Germanium, and Titanium Complexes of the E. coli Siderophore Enterobactin. *Chem. - Eur. J.* **2013**, *19* (32), 10536−10542.

(55) Pereira, L.; Mehboob, F.; Stams, A. J. M.; Mota, M. M.; Rijnaarts, H. H. M.; Alves, M. M. Metallic nanoparticles: microbial synthesis and unique properties for biotechnological applications, bioavailability and biotransformation. *Crit. Rev. Biotechnol.* **2015**, *35* (1), 114−128.

(56) Yan, B.; Wrenn, B. A.; Basak, S.; Biswas, P.; Giammar, D. E. Microbial Reduction of Fe(III) in Hematite Nanoparticles by Geobacter sulfurreducens. *Environ. Sci. Technol.* **2008**, *42* (17), 6526−6531.

(57) Bosch, J.; Heister, K.; Hofmann, T.; Meckenstock, R. U. Nanosized iron oxide colloids strongly enhance microbial iron reduction. *Appl. Environ. Microbiol.* **2010**, *76* (1), 184−189.

(58) Römheld, V. The role of phytosiderophores in acquisition of iron and other micronutrients in graminaceous species: An ecological approach - Springer. *Plant Soil* **1991**, *130* (1), 127−134.

(59) Renshaw, J. C.; Robson, G. D.; Trinci, A. P. J.; Wiebe, M. G.; Livens, F. R.; Collison, D.; Taylor, R. J. Fungal siderophores: structures, functions and applications. *Mycol. Res.* **2002**, *106* (10), 1123−1142.

(60) Johnstone, T. C.; Nolan, E. M. Beyond iron: non-classical biological functions of bacterial siderophores. *Dalton Trans.* **2015**, *44* (14), 6320−6339.

(61) Duckworth, O. W.; Akafia, M. M.; Andrews, M. Y.; Bargar, J. R. Siderophore-promoted dissolution of chromium from hydroxide minerals. *Environ. Sci. Process. Impacts* **2014**, *16* (6), 1348−1359.
(62) Akafia, M. M.; Harrington, J. M.; Bargar, J. R.; Duckworth, O. W. Metal oxyhydroxide dissolution as promoted by structurally diverse siderophores and oxalate. *Geochim. Cosmochim. Acta* **2014**, *141*, 258−269.

# Supporting information

# Remote biodegradation of Ge-imogolite nanotubes controlled by the iron homeostasis of *Pseudomonas brassicacearum*

*A. Avellan,[1,2,3] * M. Auffan,[1,2] A. Masion,[1,2] C. Levard,[1,2] M. Bertrand,[3] J. Rose,[1,2] C. Santaella[2,3] and W. Achouak [2,3]*

(1) *Aix-Marseille Université, CNRS, IRD, CEREGE UM34, 13545 Aix en Provence, France.*

(2) *iCEINT, International Center for the Environmental Implications of NanoTechologies, CNRS - Duke university, Europôle de l'Arbois, 13545 Aix-en-Provence, France.*

(3) *Laboratory of Microbial Ecology of the Rhizosphere and Extreme Environments (LEMIRE), Aix-Marseille Université, CEA, CNRS, UMR 7265 Biosciences and biotechnology Institute of Aix-Marseille (BIAM), ECCOREV FR 3098, CEA/Cadarache, 13108 St-Paul-lez-Durance, France*

* Corresponding authors: avellan@cerege.fr

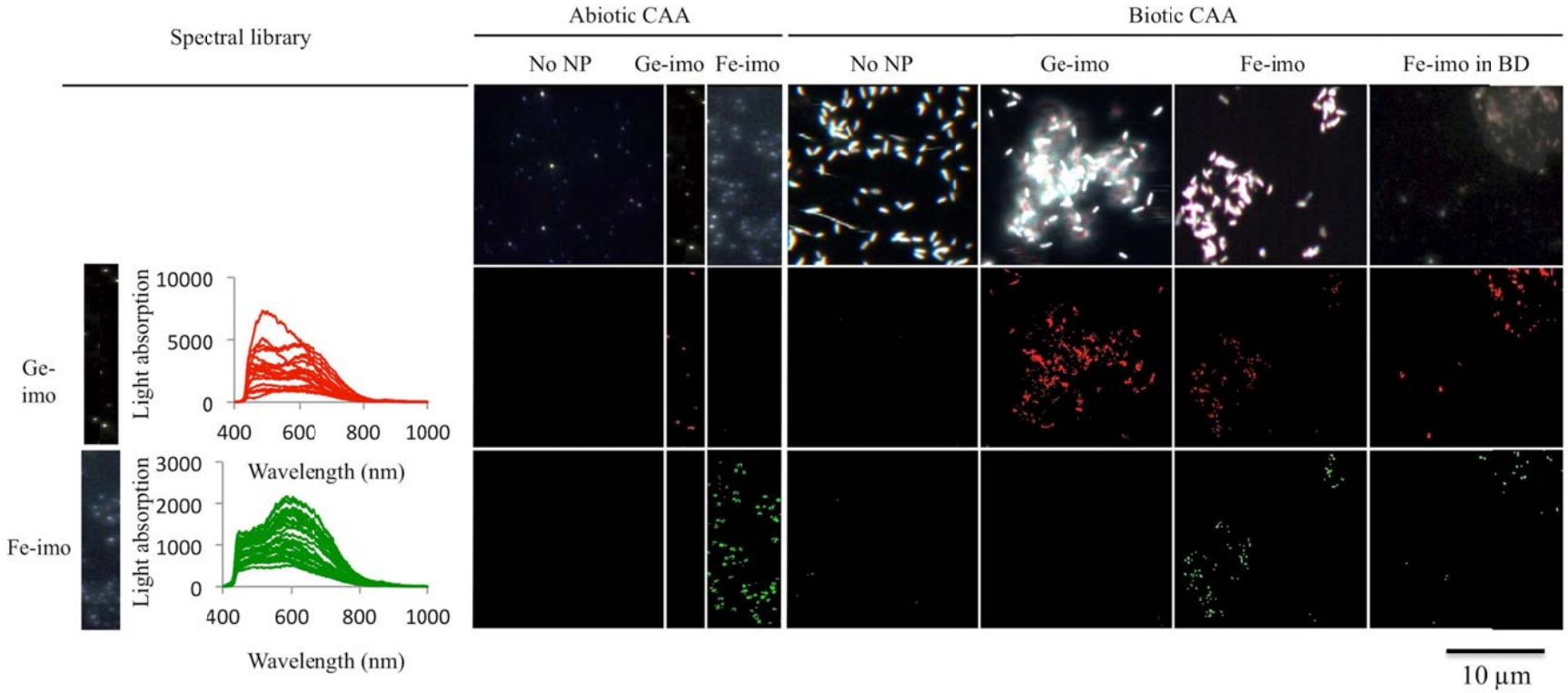


**Figure S. 1 Hyperspectral images, spectral libraries and SAM results of Ge-imo and Fe-imo in CAA media. Ge-Imo or Fe-imo incubated in abiotic media were used to build respective spectral libraries. These libraries were used to process spectral angle mapping (spectral angle of 0.085rad). Pixel with spectral signature similar to specific NP spectral signature are highlighted in red (Ge-imo signature) or in green (Fe-imo signature). Note that No Ge/Fe-imo signal were founded in biotic nor abiotic CAA without NP.**

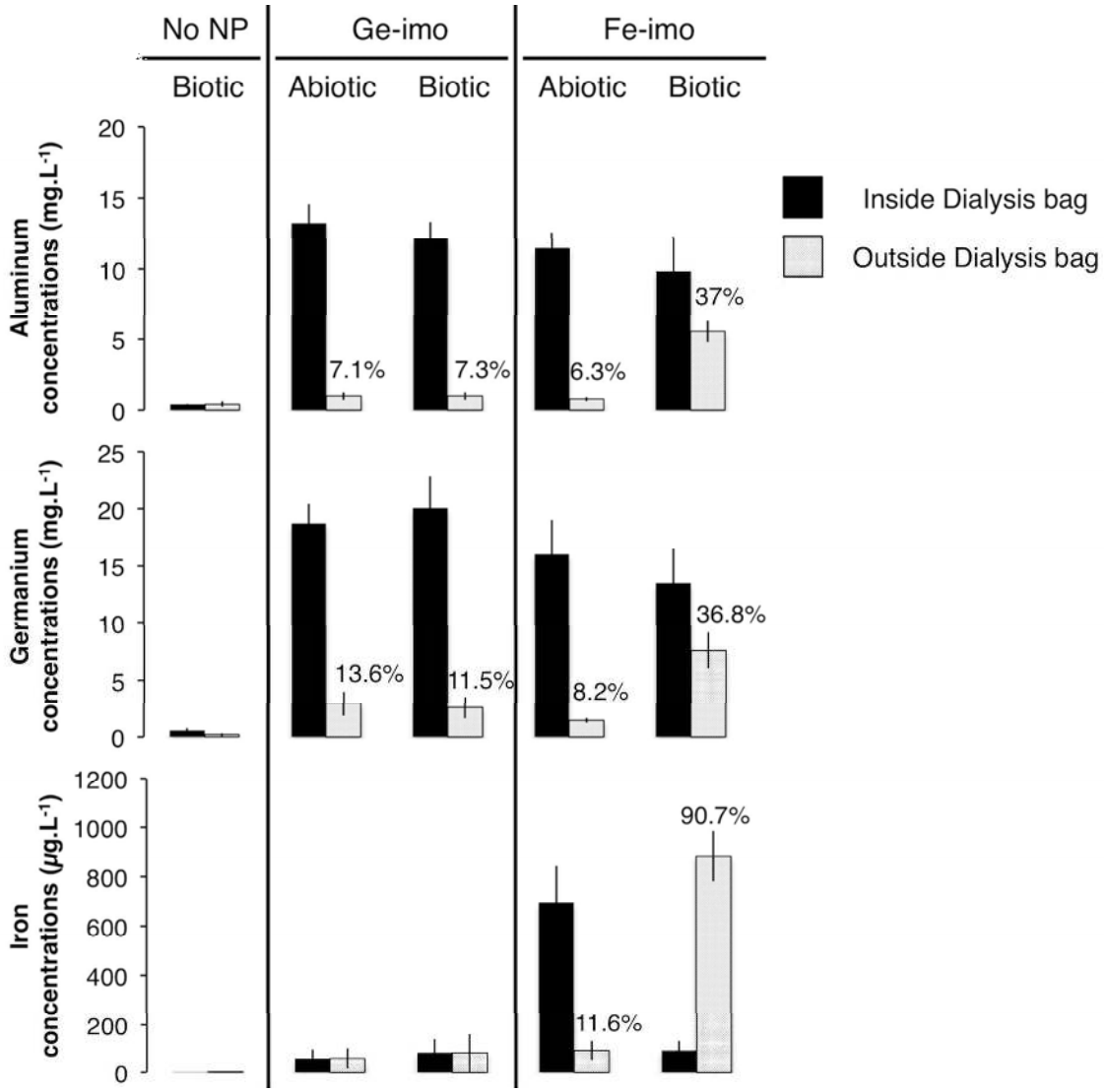


**Figure S. 2 : Al, Ge and concentrations in abiotic and biotic CAA media with or without NP in non-direct contact with *P. brassicacearum* scenarios. Measurements have been made both inside or outside the dialysis bag and the percentage of element released outside the dialysis bag were calculated.**